ELSEVIER

Surface Science 410 (1998) 290–311

surface science

Growth, morphology, and crystalline structure of ultrathin Fe films on $Cu_3Au(100)$

M.-T. Lin *, J. Shen, W. Kuch, H. Jenniches, M. Klaua, C.M. Schneider, J. Kirschner

Max-Planck-Institut für Mikrostrukturphysik, Weinberg 2, D-06120 Halle, Germany

Received 2 June 1997; accepted for publication 9 February 1998

Abstract

The growth mode, morphology, and crystalline structure of Fe films on $Cu_3Au(100)$ are studied for different growth temperatures (300 and 160 K), using in situ scanning tunneling microscopy and low energy electron diffraction. Multilayer growth is found to be predominant for both growth temperatures. Only in films of 3–4 monolayers (ML) grown at 300 K is a mixed mode of layer-by-layer growth and island growth observed. An fcc-to-bcc structural transformation, accompanied by a distinct change in the surface topography, starts at about 3.5 ML and 5.5 ML for the growth temperatures of 300 and 160 K, respectively. For both growth temperatures bcc-like Fe in $Fe/Cu_3Au(100)$ assumes, most likely through a Bain path, a surface plane with the (100) rather than the (110) orientation found in the Fe/Cu(100) system. Both the surface morphology and the onset thickness of the fcc–bcc structural transformation are shown to be strongly affected by the growth temperature. © 1998 Elsevier Science B.V. All rights reserved.

Keywords: Crystalline structure; $Cu_3Au(100)$; Fe; Low energy electron diffraction; Magnetism; Morphology; Scanning tunneling microscopy; Thin film growth

1. Introduction

The interplay between morphology, structure, and magnetic properties has recently become one of the main interests in the study of magnetic thin films. The magnetic properties in thin film systems often appear to be conditioned by crystalline structure and morphology, which in turn depend sensitively on the preparation conditions such as the growth temperature and the substrate. In particular, fcc-like Fe films have been extensively investigated in recent years owing to the diverse interrelations between magnetic properties and structure as well as morphology. This manifests itself essentially in two important aspects: The first concerns the dependence of the magnetic phase on the lattice parameter [1–3]. For example, in Fe/Cu(100) films grown at 300 K, varying the film thickness or changing the growth temperature, the (fct–fcc) structural evolution has been shown to be responsible for a magnetic phase transition from the ferromagnetic to the antiferromagnetic (or paramagnetic) phase [4,5]. The structural evolution gives rise to a change of the lattice parameter, leading to the magnetic phase transition. This behavior is mainly attributed to the critical value of the Cu lattice constant (3.61 Å), which lies midway between those of the ferromagnetic phase

* Corresponding author. Present address: National Taiwan University, Department of Physics, Taipei, Taiwan. E-mail: mtlin@phys.ntu.edu.tw

0039-6028/98/$19.00 © 1998 Elsevier Science B.V. All rights reserved.
PII: S0039-6028(98)00325-2

(3.64 Å from Ref. [1]) and the antiferromagnetic phase (3.59 Å from Ref. [6]) of fcc-like Fe. By using an alternative substrate such as $Cu_3Au(100)$ [7], having a larger lattice constant (3.75 Å), the fcc-like Fe films exhibit the ferromagnetic phase only, independently of the growth temperature [7,8]. So far, this aspect is theoretically and experimentally reasonably well understood, as indicated above by Refs. [1–8].

The second aspect is the influence of the structural and morphological properties, such as the structural transformation and the interface or surface roughness etc. on the magnetic anisotropies and especially on the spin reorientation transition. In Fe/Cu(100), it has been observed that the reorientation transition of the magnetization vector from a perpendicular to an in-plane direction is associated with an fcc–bcc structural transformation [4]. Nevertheless, the extreme sensitivity of the magnetic phase in this system to the crystalline structure makes it difficult to extract possible influences of other morphological and structural factors on the magnetic properties. It is therefore necessary to have a more stable magnetic phase, as observed in fcc-like $Fe/Cu_3Au(100)$ films [7,8], in order to investigate the influence of (fcc to bcc) structural transformations and the surface roughness on the magnetism.

Therefore, we performed a study of the growth, morphology, and structure of Fe films on $Cu_3Au(100)$ at different growth temperatures, using scanning tunneling microscopy (STM), low energy electron diffraction (LEED), and medium energy electron diffraction (MEED). This study provides the essential knowledge of structure and morphology for the identification of their interrelation with the magnetic properties.

In Section 2 the experimental details are described. In Section 3 we focus on the particular properties of the $Cu_3Au(100)$ substrate which may be important factors in determining the growth mode and the surface morphology of the film. Results of the STM studies and the LEED measurements are shown in Section 4. Section 5 combines the discussion of the growth mode, the findings on the film topography, and the fcc–bcc structural transformation with a comparison with the Fe/Cu(100) system. A brief discussion of the effect of structural transformation and roughness on magnetic properties will also be given in Section 5.

2. Experimental

The experiments were carried out in situ in three different UHV chambers (base pressure 2×10^{-8} Pa). The investigation of the crystalline structure of the sample was undertaken in a UHV system equipped with facilities for LEED, Auger electron spectroscopy (AES), and thin film growth. A face-to-face arrangement of the LEED system and the AES system permits the MEED measurement in a grazing incidence geometry, by recording the intensity of the specular electron beam displayed on the LEED fluorescent screen. To monitor the process of film growth, MEED with an incidence angle of less than 5° was employed during the evaporation of iron. Studies of the surface morphology were carried out in another UHV system equipped for STM and AES, and with iron evaporators. The scanning tunneling microscope involved a special design, such that the films could be deposited without removing the sample from the STM position [9]. Our scanning tunneling microscope is thus able to follow the process of film growth in the very same region of the surface. Since this scanning tunneling microscope works only at room temperature, this special capability is limited to the case of the film growth at room temperature. For film growth at low temperature, we use another STM system, where the sample was first cooled on a manipulator and after deposition transferred into the scanning tunneling microscope. All STM images were taken in the constant current mode at positive or negative sample bias voltage of about 1.0 V and a tunneling current of about 1.0 nA.

The pressure during Fe deposition was kept below 5×10^{-8} Pa at an evaporation rate of about 1 ML min^{-1}. Fe films were grown at two temperatures, 300 and 160 K. The sample temperature was carefully controlled within a range of ±5 K. The films grown at 160 K were briefly annealed at 300 K before measurement in order to ensure a film preparation procedure comparable with that

of other low-temperature grown films used in the magnetic measurement. According to our primary study [10], however, significant effects of annealing at 300 K on the film morphology and the critical thickness for the spin reorientation were not observed.

For the structural investigation of the films LEED $I(E)$ measurements were performed. A full interpretation of a LEED $I(E)$ curve is in general more involved than can be done within a kinematic theory. Information on the average vertical interlayer distance, however, can already be extracted from the LEED $I(E)$ curves taken for the (0,0) diffraction beam, by considering a constructive interference condition for the electron wave (Bragg condition) within the kinematic analysis. The vertical interlayer distance $a_\perp$ can then be expressed as:

$$a_\perp(n) = \frac{np\hbar}{\sqrt{2m(E_p + V_0)}\sin h}. \quad (1)$$

Here, the integer n is the order of the corresponding interference, E_p the primary energy of the electron, V_0 is the additional energy shift due to the average inner potential in the crystal, m is the electron mass, and h is the incident angle with respect to the sample surface. h is 4° in our measurements, and the [001] direction of the crystal surface lies in the reflective scattering plane of the electron beam. $a_\perp$ is determined by a linear regression of E versus $n2$. This method has been successfully applied in Fe/Cu(100) [11,12] for monitoring the average vertical interlayer distance as a function of temperature.

The substrate used for growing Fe films was a disk-shaped $Cu_3Au(100)$ single crystal. It was initially treated by cycles of Ar^+ ion sputtering (20 min at 1.5 keV) and annealing (15 min at 900 K) for a period of about 50 h. After this procedure the bulk contaminants (mainly carbon and sulfur) had reduced below 2% of a monolayer as checked by AES. Prior to deposition of the Fe films the $Cu_3Au(100)$ crystal was cleaned by 1.5 keV Ar^+ ion bombardment and annealed to 900 K for 2 min. In addition, in order to restore the chemical ordering of the alloy substrate, it was tempered at 600 K for 30 min. ($Cu_3Au(100)$ exhibits a chemical order/disorder transition at ~660 K [13]). After such a treatment the LEED pattern of the substrate revealed a clear $c(2\times2)$ superstructure which is usually observed in a well-ordered $Cu_3Au(100)$ crystal. In the next section we will give a more detailed description of the particularities of the $Cu_3Au(100)$ alloy crystal surface which may influence the film growth.

3. Particularity of the $Cu_3Au(100)$ substrate

Fig. 1a shows the LEED pattern of the $Cu_3Au(100)$ alloy substrate prepared as described above (i.e. 30 min additional tempering at 600 K). It reveals a $p(1\times1)$ symmetry and a clear $c(2\times2)$ superstructure. The $c(2\times2)$ superstructure is due to the L_{12}-type lattice below the chemical order/disorder transition temperature of 660 K, which can be visualized by an fcc unit cell with gold atoms at the cube corners, and copper atoms in the center of each face of the cube (see Fig. 1b). Above the transition temperature the crystal structure may be described as a simple fcc lattice with 75% (25%) probability to find a Cu (Au) atom at a given lattice site, resulting in a $p(1\times1)$ LEED pattern.

Assuming a simple truncation of the bulk crystal, a well-ordered $Cu_3Au(100)$ surface has two possible atomic arrangements: (i) a pure Cu surface, and (ii) a Au-rich surface with 50% gold concentration (Cu–Au surface). In a previous high energy ion scattering experiment [14] the composition ratio Au/Cu of the topmost layer was determined to be close to unity. A strong preference of a mixed Cu–Au surface termination and the predominant appearance of bilayer steps were also reported by Niehus et al. in a study using low energy ion scattering and in an atomic resolution STM experiment [15]. It must be noted that in order to restore the chemical ordering, the samples used in Refs. [14,15] were prepared by an extensive annealing procedure (20 h at ~450 K or 4 h at ~650 K in Ref. [14], 10 h at 500 K in Ref. [15]).

Since details of the surface topography such as the extension of the terraces, existence of bilayer

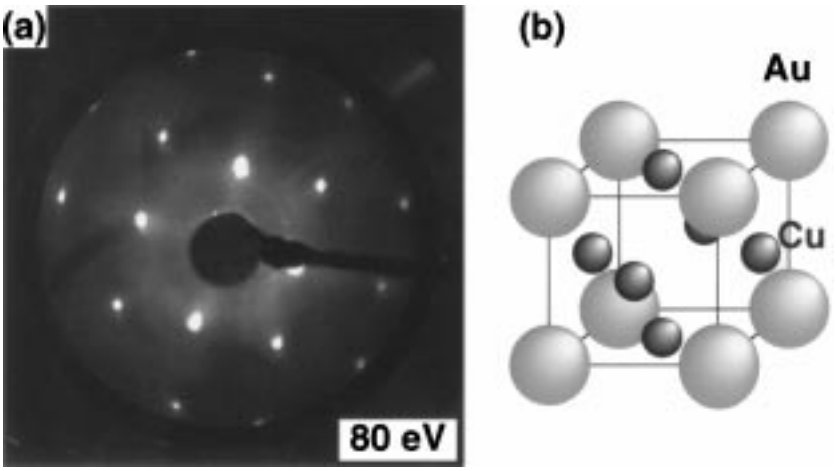

Fig. 1. (a) The LEED pattern of clean ordered $Cu_3Au(100)$ and (b) its crystallographic model. The $c(2\times2)$ superstructure indicates the chemical order of the alloy substrate.

or monolayer steps, and the chemical composition of the substrate surface may have a decisive influence on the film growth, it is important to obtain a better characterization of the $Cu_3Au(100)$ substrate used in our work, and to develop a suitable preparation process. To investigate the effect of the annealing time, the results of three different preparation procedures were compared regarding the chemical ordering and the topography of the crystal surface: After sputtering and 2 min of annealing at 900 K the sample was annealed at 600 K for (a) 30 min, (b) 6 h, or (c) with the help of liquid nitrogen cooled to 300 K in 5 min without annealing at 600 K. For all three procedures, a clear $c(2\times2)$ superstructure on the LEED pattern was observed. Only after procedure (c) did the surface reveal a considerably weaker intensity of the (1/2,1/2) superstructure spots, while in the other two cases the intensity was nearly the same. This indicates that our crystal prepared after any of these three procedures revealed at least a partially developed chemical order.

The average extension of the terraces in our STM images is of the order of 500 Å, which is about a factor of 5 larger than that shown in Ref. [15]. This value did not change significantly in the above three cases, indicating that the annealing at 600 K does not have a crucial influence on the dimensions of the terraces. The STM measurements of our crystal exhibit a preferred terrace edge orientation along [011] in all three preparation processes, in agreement with Ref. [15].

Fig. 2a shows the STM image of the substrate surface prepared by procedure (a). The line scan profile in Fig. 2b marks the presence of both monolayer and bilayer steps. As shown schematically for an ideally ordered $Cu_3Au(100)$ in Fig. 2c, two surface planes (or terraces) separated by a bilayer step should have the same chemical configuration (either a pure Cu or a Cu–Au surface), and those separated by a monolayer step must have different surfaces. To address this aspect, however, it is necessary to recall the role of surface segregation in $Cu_3Au(100)$ below and above the order–disorder transition temperature (660 K), which was theoretically predicted by atomistic simulations [16] or semi-infinite lattice-gas models [17], and was reported by experimental results of X-ray scattering [18]. It results in an increase of the Au concentration in the layers close to the surface, leading to a mixture of the ordered and disordered phase even at room temperature. A further indirect indication in our STM data which may help us to identify the surface with a mixed chemical configuration is the following finding: Some STM images reveal bias-voltage dependent image qualities for the terrace surfaces separated by monolayer steps, indicating different chemical

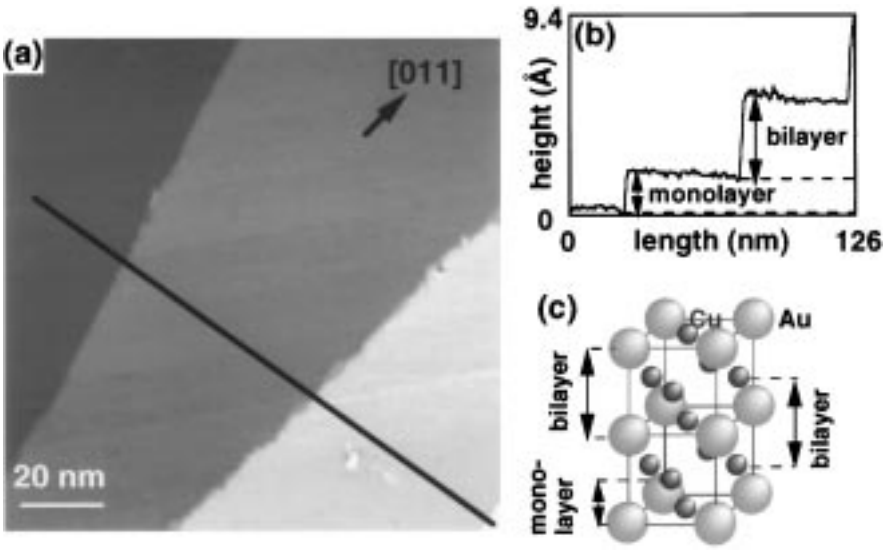

Fig. 2. (a) STM image of an ordered $Cu_3Au(100)$ surface. There is a preferred terrace orientation along [011]. (b) The line scan profile indicates two different step heights: a monolayer and two bilayer steps. As shown in (c) the schematic picture of the $Cu_3Au(100)$ crystal, two terraces separated by a monolayer step should have different chemical configurations on the surface, while those separated by a bilayer step should have the same surface termination.

configurations of these surfaces1. For the terrace surfaces separated by bilayer steps we did not find any significant difference in STM image qualities. Therefore, with the help of this finding we can still separate terraces with different configurations by distinguishing monolayer or bilayer steps, although we cannot determine what kind of surface configuration an individual terrace has. The surface terminations may be, for example, only partially ordered, i.e. partially ''Cu'' and ''Cu–Au'' surfaces due to the surface segregation of Au.

In our STM data, both bilayer and monolayer steps were always found even after 6 h annealing at 600 K. In these STM images the areas of terraces with two different surface configurations were measured. The area ratio between two different terminations amounts to 1.56, 1.51, and 1.05 for the cases with 30 min, 6 h annealing at 600 K, and fast cooling, respectively. The first two values, which are greater than unity and close to each other, indicate that the crystal surface prefers a certain surface termination and reaches almost the same chemical order after 30 min of annealing at 600 K with respect to the surface microtopography. A further annealing process did not improve the chemical order and the surface configuration beyond this state. This is why the $Cu_3Au(100)$ crystal used for the film growth in this work was reordered for 30 min rather than for several hours, saving considerably preparation time.

Since Au in the bulk has a lower surface free energy (1.6 J m^{-2}) than Cu (1.9 J m^{-2}) [19–21], a different concentration of Au on the substrate surface may give rise to a different growth mode. In order to follow the Fe growth for different surface terminations, the scanning range for growth at 300 K was intentionally chosen, as shown in Fig. 2a, to include both monolayer and bilayer steps, and consequently different surface terminations. Based on the above discussion, the left two terraces, separated by a monolayer step, are thus expected to have different surface configurations. It will be shown later in the next section that no distinct difference in growth mode and

1 This effect is due to a certain ''instability'' of the tip at variation of the sample bias or during scanning, which may catch some individual particles for some time. Such an unstable tip, which is often found at the beginning of the measurement, may give rise to some sensitivity to the different electronic configurations of terraces.

morphology of Fe films on these two different surface configurations is found.

4. Experimental results and analysis

4.1. Topography of Fe/Cu_3Au(100) films

4.1.1. Growth at 300 K

In our previous paper [7] we have identified from MEED experiments for growth at 300 K of the Fe film three thickness regions with different growth behavior. In order to make contact with the MEED curve in Ref. [7], the STM images for growth at 300 K are also presented for these three regions: the initial stage of growth before the first relative maximum in MEED intensity (0–2.5 ML, region A), two maxima with the same intensity (2.5–4.5 ML, region B), and the thickness range with the decreasing MEED intensity (>4.5 ML, region C). Later, we will also compare the results of both STM and MEED experiments.

4.1.1.1. Region A: 0–2.5 ML. Fig. 3 shows the STM images taken on a 100 nm × 100 nm scale for Fe coverages of 0.4, 1.1, 2.2, and 2.5 ML. We see the three terraces separated by a monolayer step and a bilayer step as mentioned above. The left two terraces should include two different surface configurations of Cu_3Au(100). Up to 0.4 ML iron grows in a high nucleation density mode (224 000 islands mm^{-2}) with an average island size of 1.3 nm^2 at 0.4 ML, smaller than that of Fe/Cu(100) films grown at 300 K [22]. The layer filling of the second layer at this coverage is 4% of the whole observed area.

At a coverage of 1.1 ML, the layer filling of the first layer reaches only 68%, while that of the second layer is already 30%. One can also see several third layer islands (the brightest parts on each terrace). Note that the islands become larger but are still separated from each other, far away from percolation of the first layer. A significant part of the substrate surface is still exposed. The films up to this coverage clearly reveal a multilayer growth. At higher coverages of 2.2 ML and 2.5 ML, the Fe islands become much larger and their shape indicates a preferential growth oriented along ⟨011⟩. Following the island growth at both coverages of 2.2 ML and 2.5 ML, one sees that islands prefer to coalesce with other islands in the ⟨011⟩ orientation, while there is a tendency to remain disconnected in the ⟨001⟩ orientation. Comparing the images of coverages up to 2.5 ML on the left two terraces, which, as mentioned above, should have different surface terminations, we do not observe differences in the surface topography for the two different surface terminations. The Fe films on all terraces show a multilayer growth with a preferential coalescence orientation ⟨011⟩, indicating no influence of the different chemical configurations of different terraces on the film growth. Also no difference between films growing along monolayer steps and along bilayer steps is found. According to our AES data and STM images taken at different bias voltage, we find no evidence of interdiffusion in the initial nucleation stage[2]. This could be why we find no substantial difference in the Fe growth on the two different terrace termination.

4.1.1.2. Region B: 2.5–4.5 ML. Fig. 4a–c shows STM images of Fe films at coverages of 3.0, 3.5, and 4.0 ML. At 3.0 ML (Fig. 4a) the first and second layers are almost completely filled (the tiny darkest parts on each terrace). In this image mainly the third and the fourth layers are exposed (the second brightest and the brightest part on each terrace, see also gray scale referring to the middle terrace indicated in Fig. 4). The third layer is nearly completed (about 82% layer filling[3]). The fourth layer appears as islands (31% layer filling). The line scan profile gives a height of the Fe layer of (1.9 ± 0.2) Å, which corresponds to the vertical interlayer spacing of the substrate. This indicates an fcc-like structure of the Fe layers at this coverage. Note that the regular shape of the Fe islands found at lower coverages is still well developed.

Some small irregular patches on the topmost

[2] In this case, the surface segregation is expected to be very sensitive to the growth temperature and may occur already at a slightly higher temperature than room temperature.

[3] The layer fillings are determined by taking a histogram of the height distribution from the STM images and counting the relative area (percentage) with the corresponding layer height with respect to the total area investigated.

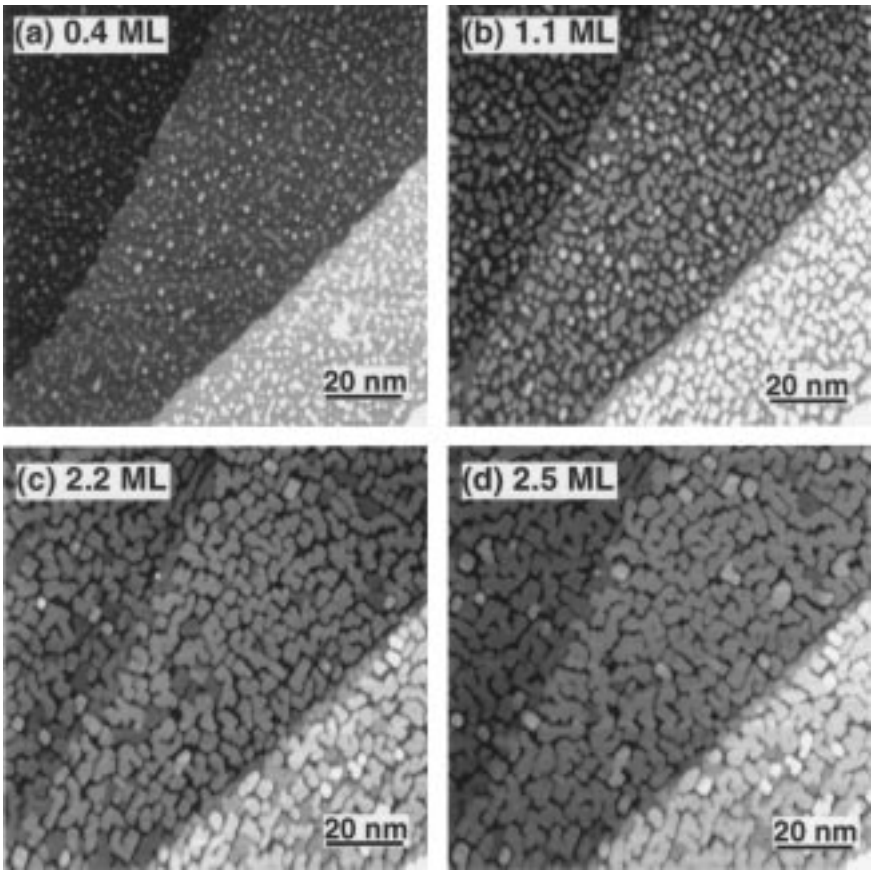

Fig. 3. STM images of (a) 0.4 ML, (b) 1.1 ML, (c) 2.2 ML, and (d) 2.5 ML Fe on $Cu_3Au(100)$ for growth at 300 K. Note that Fe islands at coverages starting from 2.2 ML reveal a regular shape with a preferred $\langle 011 \rangle$ orientation.

islands are observed at a coverage of 3.5 ML. They are seen for the first time at that coverage (Fig. 4b). The line scan profile shown in Fig. 4d reveals two typical heights: (1.9 ± 0.2) Å and (0.5 ± 0.2) Å. The fractional value of the latter indicates some distorted structure, possibly attributed to dislocation or buckling of the Fe film. These irregular Fe patches can be expected to indicate the onset of some kind of fcc–bcc structural transformation, which must appear above a certain coverage according to basic thermodynamic considerations [22]. We can obtain further structural information by taking the height distribution of two areas denoted A and B, as indicated in Fig. 5, which is a magnification of Fig. 4b. The area A includes the regular Fe layers (gray and black), and an irregular Fe patch (white gray) associated with the 0.5 Å fractional height in the line scan profile in Fig. 4d. The histogram of the height distribution taken over the area A indicates two different layer distances: 1.9 Å and 1.5 Å. The former is, as indicated in the line scan of Fig. 4d, the value corresponding to the fcc-like layers. The latter can be identified with the bulk interlayer distance of (100)-oriented bcc Fe. In contrast, area B is chosen across the edge of the bilayer step. The layer distance between the regular Fe layers located at the upper and the lower terrace is shown to be 3.8 Å, being consistent with the height of a bilayer step on the $Cu_3Au(100)$ surface (see also Fig. 2).

As compared with the 3.5 ML film, the irregular Fe patches at 4.0 ML become larger and more numerous and reveal an irregular shape (Fig. 4c),

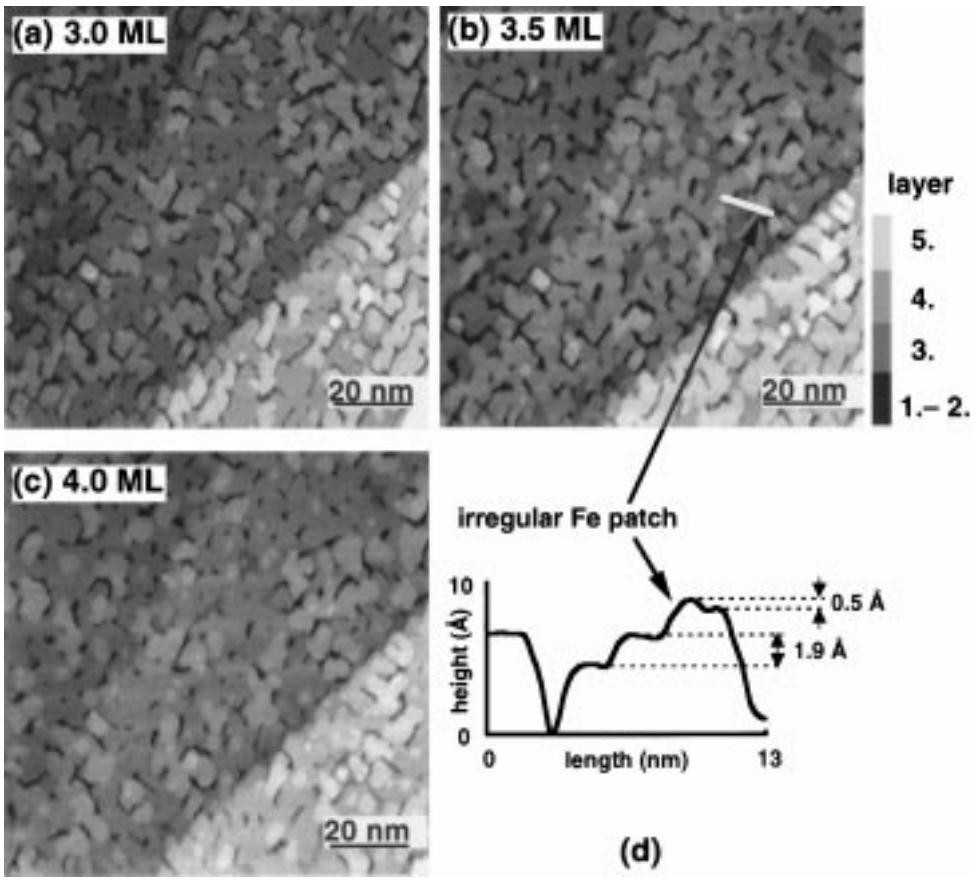

Fig. 4. STM images of (a) 3.0 ML, (b) 3.5 ML, and (c) 4.0 ML Fe films on $Cu_3Au(100)$ for growth at 300 K; (d) the height profile along the line indicated in (b). The gray scale is used to indicate the corresponding layer on the middle terrace. Two values of step heights are found in (d): 1.9 Å for the regular island and the fractional height of 0.5 Å.

in contrast to Fe islands at lower coverages. At this coverage, however, one can still see the regular island shape with the ⟨011⟩ orientation despite many irregular Fe patches grown on the topmost layer of the film.

4.1.1.3. Region C: coverages higher than 4.5 ML. In Fe films of 4.9 and 5.4 ML (Fig. 6) the irregular Fe patches dominate the surface topology so that the surface is rougher than that of the 3–4 ML films. At 5.4 ML, none of the regular Fe islands which are characteristic for the lower layers are observed. Fe films of even higher coverages investigated (up to 9 ML) reveal a surface topography similar to those of 5.4 ML. All the height distributions taken at higher coverages (4.0 ML and 4.9 ML) show the layer height of the irregular patches to be 1.5–1.6 Å. This supports our hypothesis that the fractional height of Fe patches marks the onset of a structural transformation, and suggests furthermore that the irregular Fe patches can be referred to a bcc-like phase with (100) orientation. (Note that since an ''fcc'' or ''bcc'' structure needs at least three layers to be defined, we refer to the irregular Fe patches as a bcc-like phase in the sense that their neighboring layer distance can be identified with that of a bcc structure.)

Finally, the layer filling versus the total coverage is plotted in Fig. 7 for all coverages investigated. This graph gives quantitative information about the layer distribution of the films. After the depos-

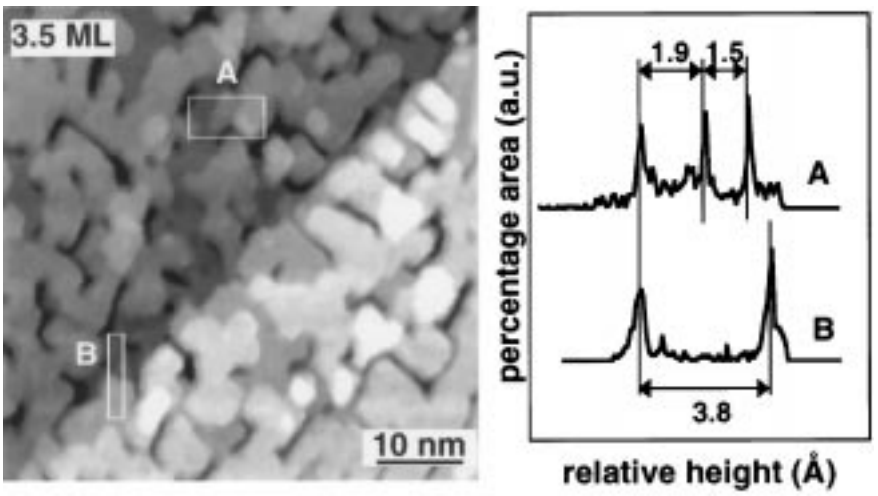

Fig. 5. Part of the STM image shown originally in Fig. 4(b), but on an enlarged scale. The height distribution plots on the right-hand panel stem from the two areas denoted A and B, as indicated by white rectangles in the STM image. The area A is particularly chosen to include the regular Fe layers (gray and black) as well as an irregular Fe patch (white gray). The histogram of the height distribution taken over the area A results in two different layer distances: 1.9 Å and 1.5 Å, corresponding to the values of the vertical interlayer distances of fcc-like Fe(100) and bcc-like Fe(100), respectively. The layer distance 3.8 Å obtained in the area B is consistent with the height of a bilayer step on the $Cu_3Au(100)$ surface.

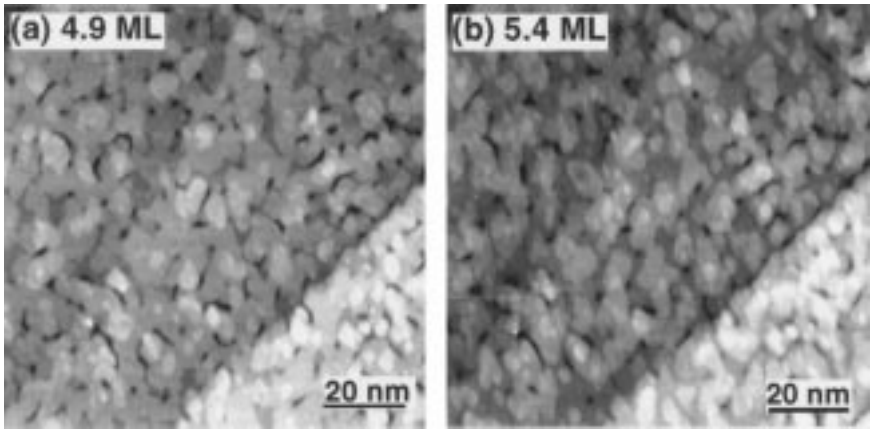

Fig. 6. STM images of (a) 4.9 ML, (b) 5.4 ML Fe films on $Cu_3Au(100)$ for growth at 300 K. The film surface is covered by irregular Fe islands, and the regular Fe layers are almost not visible.

ition of only $\sim$0.4 ML, already the second layer islands start to nucleate. At 1 ML total coverage the first layer is only 68% filled and the missing 32% of material have formed second (30% layer filling) and third layer (2% layer filling) islands. At 2 ML the second layer is only 70% completed and the third layer has already a 40% layer filling. The first layer is still uncompleted. This simultaneous growth of three layers is characteristic for films thinner than 3 ML. Going to 3 and 4 ML, one finds a higher filling of the third and fourth layer, (more than 80%), indicating a transition to a quasi layer-by-layer growth mode, as indicated by the MEED measurement (cf. Ref. [7] or Fig. 18). The uncompleted lower layers and a significant amount of higher layer islands indicate,

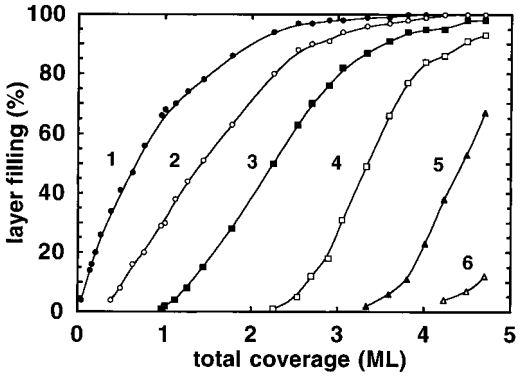

Fig. 7. Layer filling of the first six layers as a function of the total coverage for Fe/Cu_3Au(100) films grown at 300 K. Numbers 1–6 refer to the layer filling of the first to the sixth layer, respectively. At 1 ML (2 ML) total coverages the first (second) layer is only 68% (70%) filled. A simultaneous growth of three layers is characteristic for films of coverages less than 3 ML. In spite of a higher layer filling (~80%) of the third (fourth) layer at 3 ML (4 ML), the unclosed lower layers and a significant amount of higher layers indicate that this film growth is still far from an ideal layer-by-layer growth.

however, that this layer growth is still far from being ideal.

4.1.2. Growth at 160 K

Fig. 8 shows the STM images taken at 300 K from Fe films of 2.2, 4.6, 6.2, and 9.0 ML grown at 160 K. They are, in contrast to the case of growth at 300 K, not taken at the same region. At a coverage of 2.2 ML (Fig. 8a), we see mostly the third (light gray on the large terrace) and second (dark gray) layer of Fe with a layer filling of 46% and 88%, respectively. The first layer has a layer filling of ~96% and only about 4% of the substrate is exposed (both first layer and substrate are displayed in a similar gray level and are thus not distinguishable in this image.) These values of the layer filling indicate a multilayer growth, which is often observed at low temperatures owing to the reduced mobility of the adatoms. In contrast to Fe films grown at 300 K at the same coverage (see Fig. 3c), only few Fe islands coalesce in the case of growth at 160 K.

Going to 4.6 ML (Fig. 8b), the Fe islands tend to join one another and still grow without the pronounced step edge orientation found in films grown at 300 K. This leads to the formation of a random network-like morphology. Moreover, as shown in the image, such a surface morphology is found not only in the topmost layer but also in the lower layers. Hence, the coalescence of the topmost layer must already occur before the next lower layer is completely closed. At step edges this has a particular consequence. Fe islands at the edge of the terrace tend to connect with higher layer islands from a lower lying terrace. This is seen from the irregular shape of the terrace edges as compared with the clean substrate. The joined islands form an irregularly shaped network-like layer, which extends over the edge of the terrace of the substrate, thereby changing the actual position of the terrace edge. The original terrace steps of the substrate are thus obscured by the growing islands during this growth process. The new terrace edges still seem to retain the similar preferred orientation of [011] as the original terrace steps on the substrate.

The film at 6.2 ML shows an astonishingly smooth surface morphology (Fig. 8c). The sixth layer is almost completely closed, only some holes can be seen. The bright spots are islands of the seventh layer. The tendency of islands to connect to each other found at 4.6 ML can be seen as a precursor of the relatively flat surface at 6.2 ML. The surface, however, is not as smooth as is usually found for a good layer-by-layer growth. In an enlarged view (Fig. 9), the film surface exhibits a network-like fine structure with small nearly square units. This structure is only found at this coverage with an ''almost closed film'', but not at lower coverages. After a more detailed analysis, the nearly square units are determined to have a side length of 7–14 Å. The line scan profile B in Fig. 9 shows that the ridges of the network have a height of about 0.15 Å. Line scan profile A shows that a fine structure is also present along the same orientation on the top of the island of the seventh layer (bright region in the image). This indicates that the adsorbed Fe atoms are bound on the basis of this network-like structure (thus not a flat surface) and that the islands in the seventh layer keep the corrugated morphology of the sixth layer.

The film at a coverage of 9.0 ML exhibits a surface with a relatively high island density and a

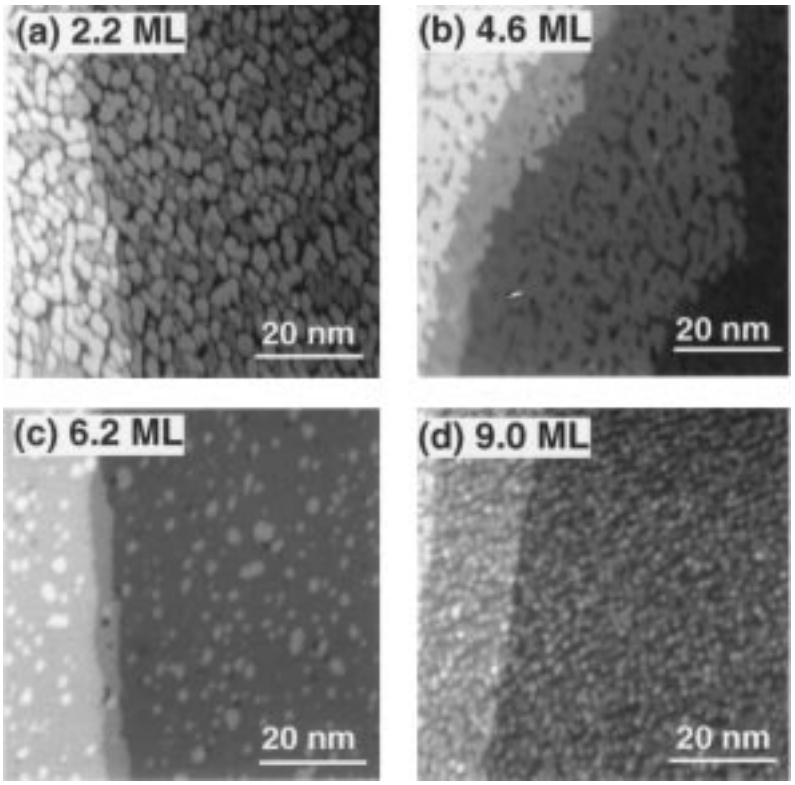

Fig. 8. STM images of (a) 2.2 ML, (b) 4.6 ML, (c) 6.2 ML, and (d) 9.0 ML Fe/Cu_3Au(100) grown at 160 K. The film at 2.2 ML clearly reveal an island growth, as usually observed at low temperature growth. At 4.6 ML, the Fe islands tend to connect each other, however, in contrast to the case of growth at 300 K, without a pronounced preferential orientation, forming a random network-like morphology. The 6.2 ML film shows an astonishingly smooth film surface, however, with a network-like fine structure, which is more clearly shown by a zoomed STM image in Fig. 9. Going to 9.0 ML, the film has a relatively high island density and a small island size, which may be attributed to the reduction of the mobility of adatoms due to the network-like fine structure observed at 6.2 ML.

small island size (Fig. 8d), in contrast to films at lower coverages. This island growth may be partially attributed to the network-like fine structure observed first at around 6.2 ML, which reduces the mobility of adatoms with respect to a flat surface, leading to a three dimensional island formation and thus a film surface with a relatively large roughness.

The height distributions obtained at coverages of 2.2 and 4.6 ML (not shown) exhibit a layer or island height of 1.9 ± 0.2 Å, corresponding to an fcc-like structure. This indicates that Fe layers (islands) up to about 5 ML still keep the fcc-registry with the substrate. At higher coverages a different behavior is found. Fig. 10 shows the height distributions taken on two different areas denoted by A and B, respectively, and indicated by the white rectangle in the STM image of the 6.2 ML thick Fe film shown in Fig. 8c.

The height distribution of area A gives an island height with respect to the almost closed layer of about 1.6 Å. This value is significantly out of registry with the Fe fcc(100) structure and close to the value of the interlayer distance of the (100) bcc phase of Fe, as found in the case of growth at 300 K. At area B, a value of the interlayer height of 1.9 Å is obtained, which is consistent with the vertical interlayer spacing of the substrate. Note that area B is intentionally chosen to include the edges of the terrace, because it is otherwise impossible to get the interlayer height of the almost closed layers. Since, as indicated above, the original

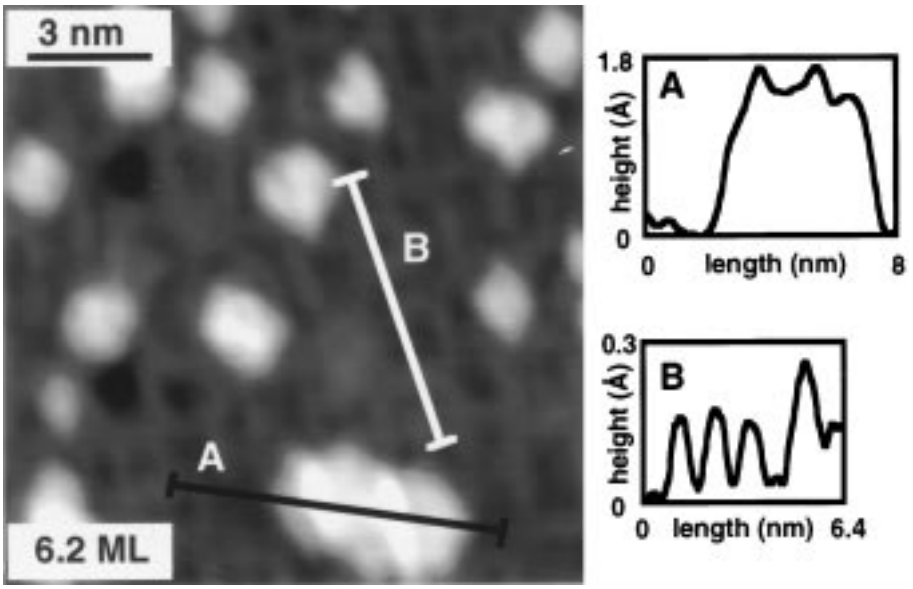

Fig. 9. The STM image of a 14 nm × 14 nm zoomed area of 6.2 ML Fe/Cu_3Au(100) grown at 160 K shown originally in Fig. 8(c). A network-like fine structure with small nearly square units is clearly observed. The profile plot on the right hand panel shows the line scan along the lines marked by A and B, which indicate a side length of 7–14 Å for the nearly square units.

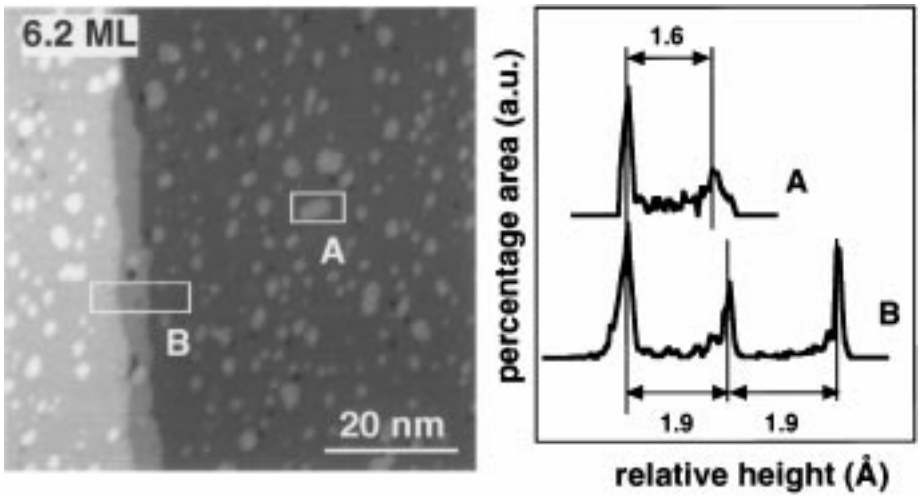

Fig. 10. Height distribution plots (right side) taken at two areas denoted A and B, as indicated by white rectangles in the STM image of 6.2 ML Fe/Cu_3Au(100) grown at 160 K shown originally in Fig. 8(c). The height distribution obtained within area A gives an island height of 1.6 Å, corresponding to the bcc-like Fe(100) structure. The value 1.9 Å obtained from area B is consistent with the vertical interlayer spacing of the fcc(100) substrate.

edge position of the substrate is obscured by the connected layers from the neighboring terraces, the terrace edge observed at 6.2 ML should represent the step height of the as-grown layers rather than that of the original terrace of the substrate. Thus the almost closed (sixth) layer at 6.2 ML still has the fcc-like phase. According to these findings at 4.6 ML and 6.2 ML, we conclude that the

fcc–bcc structural transformation should start between 5 ML and 6 ML.

4.2. Crystalline structure

4.2.1. Growth at 300 K

Fig. 11 shows the LEED pattern of 3.2 ML Fe/$Cu_3Au(100)$ grown at 300 K. The diffraction pattern reveals a $p(1\times1)$ structure similar to that of (10) spots of the substrate, indicating a pseudomorphic growth of the Fe films. The (1/2,1/2) superstructure spots, which were observed for the clean ordered $Cu_3Au(100)$ substrate (Fig. 1a), however, have disappeared. An important finding is that no superstructure due to a reconstruction of the Fe layers was observed at all coverages under investigation, in contrast with Fe/Cu(100) films grown at 300 K, where a (4×1) and (5×1) superstructure was found in the coverage regime of the perpendicular ferromagnetic phase [4]. The absence of regular reconstruction as indicated in the LEED pattern may be attributed to the high tensile strain due to an enhanced lattice mismatch

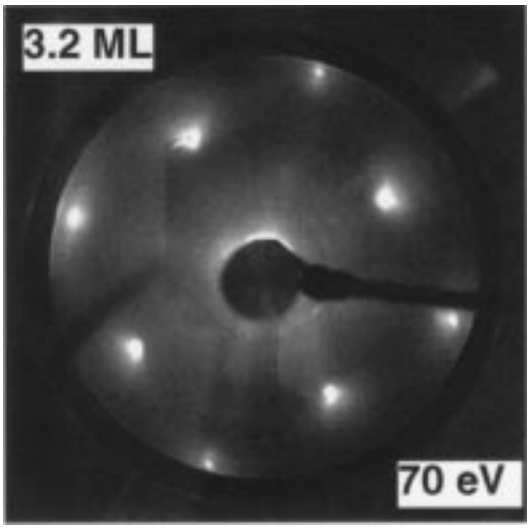

Fig. 11. The LEED pattern, taken at 160 K, of a 3.2 ML Fe film on $Cu_3Au(100)$ grown at 300 K reveal a $p(1\times1)$ structure similar to that of (1,0) spots of the substrate, indicating a pseudomorphic growth of the film. The (1/2,1/2) superstructure spots observed on the clean ordered $Cu_3Au(100)$ are obscured by the Fe film. Note that, in contrast to the findings of Fe/Cu(100), no (4×1) or (5×1) superstructure spots due to a reconstruction of the Fe film are observed.

(4.2%) in fcc-like Fe on $Cu_3Au(100)$, as compared with the case of Fe/Cu(100) (1%). A structural study of Fe_xCo_{1-x}/Cu(100) alloy thin films indicated that the compressive strain is more likely accommodated by forming a regular reconstructure than the tensile strain [23]. Moreover, the strain in our case may also be too high to be relieved merely through the minimal lateral rearrangement of the atoms (reconstruction) as found in Fe/Cu(100). Instead, numerous defects in a form of the island growth, as shown in our STM data (Figs. 3 and 4), could accommodate the strain mostly.

More quantitative structural information can be obtained from LEED $I(E)$ measurements. Fig. 12 contains a compilation of LEED $I(E)$ curves of the (0,0) diffraction beam taken at 160 K for clean $Cu_3Au(100)$ and various Fe coverages t. The solid and dotted lines indicate two different peak sequences with equal $\sqrt{E}$ distances, which correspond to two different structural phases. The indices at these lines denote the integer number of the electron wavelength associated with a constructive interference as shown in Eq. (1). The first peak sequence (solid lines) found for films at low coverages appears to be a continuation of the substrate pattern and must be related to the fcc(100)-like phase in a pseudomorphic structure on the $Cu_3Au(100)$ substrate. Its intensity decreases with increasing Fe thickness and disappears at a coverage of 7.7 ML. The second peak sequence (dotted lines) occurs in films of $\geq$3.4 ML and becomes predominant at higher coverages. Films at coverages of 3.4–5.8 ML are characterized by a coexistence of these two structural phases, at coverages larger than 7.7 ML only the second peak sequence can be observed.

Since some peaks in the LEED $I(E)$ curves which are due to multiple scattering [24] may overlap with the peaks indicated above, it is sometimes difficult to determine the exact film thickness for the onset of the second peak sequence. The method used here is to take the ratio of the intensities of the second peak sequence (or the peak with the same energy position as one of the second peak sequence) to the first peak sequence (for example, the peak around 110 eV to the peak

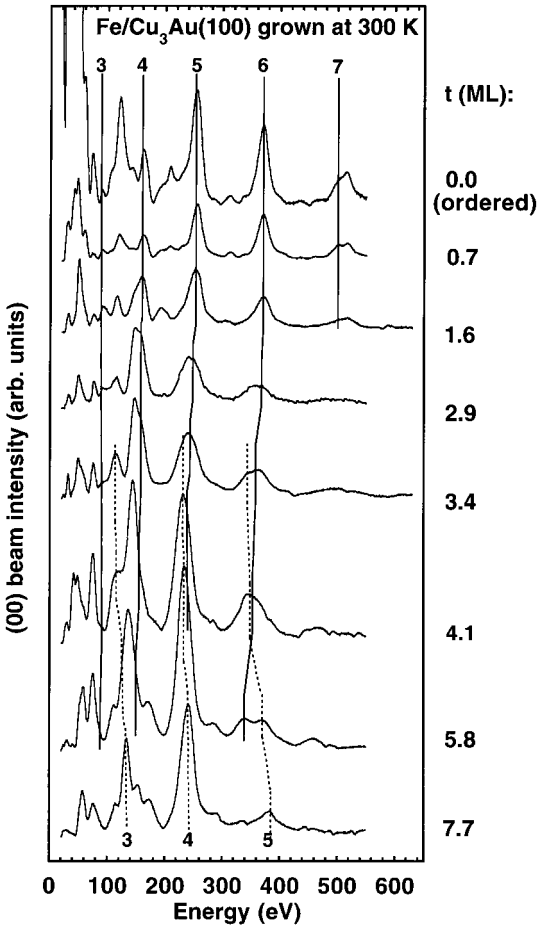

Fig. 12. LEED $I(E)$ curves of the (0,0) beam of the clean ordered $Cu_3Au(100)$ substrate and $Fe/Cu_3Au(100)$ grown at 300 K for various coverages. The solid and dashed lines indicate two different periodic peak sequences with the intensity weight depending on the thickness. The indices denote the integer numbers of the single scattering Bragg interference condition. Note that a superposition of these two peak sequences is found in the coverage range of about 3.4–5.8 ML.

of the first sequence with index 4). An increase of this ratio with the film thickness can be interpreted as the appearance of the new (second) peak sequence. The onset thickness for the second structural phase is then identified as the thickness at which the ratio defined above starts to increase with film thickness. In this way we determined the onset of the second peak sequence to be at $\sim$3.5 ML for growth at 300 K. Note that this onset thickness obtained here agrees very well with the first appearance of the irregular Fe patches as seen in the STM images above (Fig. 4b and d).

The energetic positions of the peak sequences versus the index $n2$, as an example, for 1.6 ML and 7.7 ML films are plotted in Fig. 13, which demonstrates the quality of the $\sqrt{E}$ periodicity of the ''Bragg'' maximal peaks in the $I(E)$ curves. The average vertical interlayer distances $a_{0^\perp}$ can be extracted from the slope of the straight lines by applying Eq. (1). The values of $a_{0^\perp}$ for those two peak sequences at all coverages investigated are depicted in Fig. 14. From the clean substrate we get $a_{0^\perp}=1.89\pm0.02$ Å. This is only slightly larger than the literature value of 1.875 Å [19]. The value of $a_{0^\perp}$ for the first peak sequence does not change for films up to 3.0 ML and increases only slightly at coverages above 3.0 ML, indicating a structural continuation of the fcc structure of the substrate, as mentioned above. All values of $a_{0^\perp}$ extracted from the second peak sequence are close to the interlayer distance of (100)-oriented bcc Fe ($a_{0^\perp}=1.43$ Å) rather than to that of a Fe bcc(011) structure ($a_{0^\perp}=2.02$ Å). This agrees well with the finding from the STM images.

The absence of a contracted $a_{0^\perp}$ indicates in the first place that, within the limited probing depth (about 3 ML) by this method, the atomic volume does not stay constant in pseudomorphic films. This finding somehow seems to contradict the usual expectation that in pseudomorphic films with

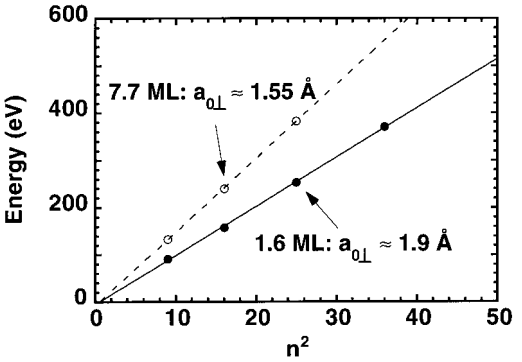

Fig. 13. Energy positions of the periodic $I(E)$ peak sequences versus the index $n2$ for $Fe/Cu_3Au(100)$ films grown at 300 K with coverages of 1.6 ML (full circles) and 7.7 ML (open circles). The values of $a_{0^\perp}$ are extracted from the slope of the straight lines applying Eq. (1).

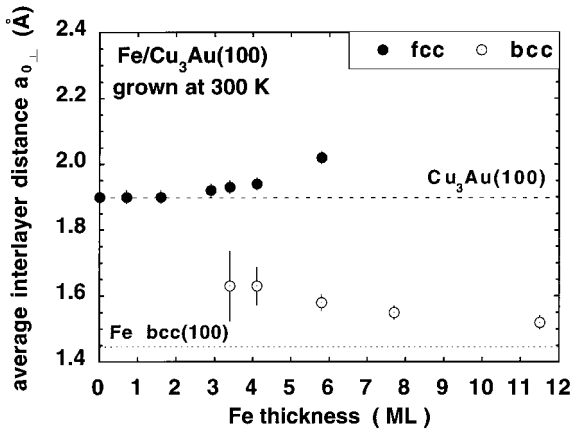

Fig. 14. Two different average vertical interlayer distances $a_{\perp}$ extracted from the two peak sequences in the $I(E)$ curves of Fig. 12. They are related to fcc-like (full circles) and bcc-like Fe (open circles), respectively. The values of the vertical interlayer distance of the $Cu_3Au(100)$ substrate (measured) and bcc(100) Fe bulk (from literature) are indicated by horizontal lines.

an expanded in-plane lattice, such as in our case, the perpendicular lattice parameter should be contracted via a Poisson ratio in order to keep the atomic volume constant [25]. This contradiction, however, may be explained if we take the complicated correlation of the lattice parameter and the magnetic moment as well as the magnetic phase in fcc-like Fe [1,2,26,27] into account. In bulk calculations, the magnetic moment of fcc-like Fe has been shown to increase with increasing lattice constant [1,2,26,27]. It is thus particularly likely for fcc-like Fe thin films to have more than one metastable atomic volume, which are connected to various ferromagnetic metastable fct states, accompanied by different magnetic moments. Recently, by using site-specific Mössbauer spectroscopy, Keavney et al. [3] have observed that the average magnetic moment of fcc-like Fe films, which were grown on $Cu_{1-x}Au_x(100)$ with varying lattice constant a_0, increases with a_0. Unfortunately, there was no comment in their work on the behavior of the corresponding vertical interlayer distance.

The STM images in Fig. 4 show that the regular Fe layers are not covered by the irregular (bcc-like) Fe patches yet do not reveal any distinct change in morphology and conserve their fcc-like structure. The coexistence of the fcc-like and bcc-like phases from 3.5 ML up to about 6 ML in the LEED data indicates further that the as-grown fcc-like Fe underlayers or parts of them still conserve their structure at least up to this coverage. Combining these findings of STM and LEED, we can thus conclude that—starting from a coverage of $\sim$3.5 ML—the bcc-like Fe patches with their irregular shape grow on top of the fcc-like islands (or layers) and progressively cover the entire surface of the fcc-like underlayers with increasing thickness, rather than different structural patterns side by side.

Finally, a pronounced structural transformation affecting the entire film such as the martensitic transformation found in Fe/Cu(100) grown at 300 K [28,29] seems not to take place here. For iron films on $Cu_3Au(100)$ up to 9 ML, the STM images show a similar surface topology to that at coverages of 4.9 ML. The structure of the underlayers under these conditions is of course barely accessible. The absence of an fcc-related peak sequence in the LEED $I(E)$ curves at higher coverages should thus be mainly attributed to the intensity attenuation of the diffracted electron beam through the bcc-like overlayers.

4.2.2. Growth at 160 K

The LEED patterns of $Fe/Cu_3Au(100)$ grown at 160 K exhibit cubic symmetry similar to that of the substrate, indicating a pseudomorphic growth in an fcc-like structure, as found in films grown at 300 K. A sequence of LEED patterns at increasing coverage show a progressive disappearance of the (1/2,1/2) spots of the $c(2\times2)$ superstructure of the substrate, which can, however, still be seen at higher coverages (see, for example, LEED pattern of 3.2 ML Fe film grown at 160 K in Fig. 15), as compared with the films grown at 300 K (cf. Fig. 11). This is attributed to island growth at low temperature, as shown in the STM images above, with more area of the substrate and of the first Fe layer still exposed than for growth at 300 K at the same nominal coverage. This leads to a smaller attenuation of the beams from the substrate. Similar to the finding in $Fe/Cu_3Au(100)$ grown at 300 K, no other superstructure (e.g. (4×1) and (5×1)) due to reconstruction of film atoms, which was observed in Fe/Cu(100) [4], is found here.

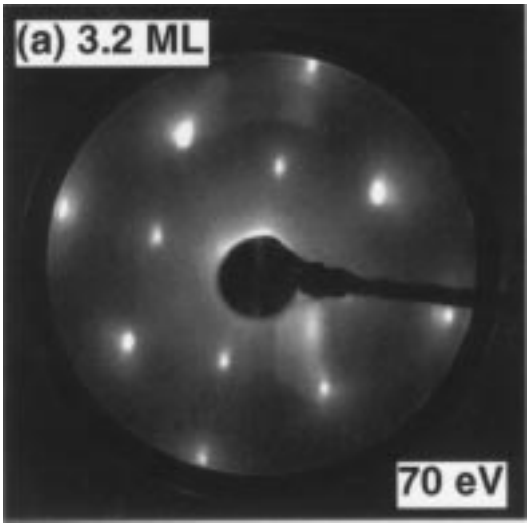

Fig. 15. The LEED pattern, taken at 160 K, of a 3.2 ML Fe film on $Cu_3Au(100)$ grown at 160 K reveal a $p(1\times1)$ structure similar to that of the (1,0) spots of the substrate, indicating a pseudomorphic growth of the film, also without any indication of (4×1) or (5×1) superstructure. Different from the case of growth at 300 K, the (1/2,1/2) superstructure spots from the ordered substrate can be still observed. This can be attributed to a smaller attenuation of the electron beam from the substrate due to an enhanced exposure area of the substrate surface in an island growth at low temperature, as compared with the room temperature growth.

Figs. 16 and 17 are plots of the LEED $I(E)$ curves, and of the interlayer distance $a_{0^\perp}$ as function of Fe thickness obtained form the LEED $I(E)$ curves. Similar to the finding in $Fe/Cu_3Au(100)$ grown at 300 K, one observes two structural phases corresponding to two different interlayer distances. The relative weights of these two structural phases depend again on the Fe thickness. At Fe thicknesses up to $\sim$5 ML the first structural phase (indicated by solid lines in Fig. 16), which is related to the fcc-like structure, is found in this region, as shown in Fig. 17, $a_{0^\perp}$ increases with the Fe thickness reaching a value of (1.98 ± 0.02) Å at 5.5 ML. At coverages higher than 3.6 ML a new peak sequence appears. The values (around 1.5 Å) of the corresponding $a_{0^\perp}$ of this second sequence are much smaller than the value for bcc(110) Fe (2.02 Å) and close to that of a bcc(100) Fe (1.43 Å), being consistent with the finding of the layer height from STM data at a coverage of 6.2 ML (cf. Fig. 10). A coexistence of both fcc-like and bcc-like structures is also found at coverages between 5 and 7 ML. Note that the (100) bcc phase starts to develop at a coverage of about 5.5 ML. This value is larger than that in $Fe/Cu_3Au(100)$ grown at 300 K.

5. Discussion

5.1. Growth mode of $Fe/Cu_3Au(100)$

Recording RHEED or MEED intensity oscillations during deposition is a widely used and convenient way of area averaging real-time growth diagnostics, while STM can take a direct image of the geometrical structure of the film surface, giving more quantitative information about local surface roughness, island density, and growth mode. In order to make contact between STM and MEED measurements, the roughness extracted from STM data is compared with the MEED specular intensity curve. In Fig. 18 both the surface mean roughness R (solid triangles) and the MEED specular intensity (solid line) are plotted as a function of Fe thickness for $Fe/Cu_3Au(100)$ grown at 300 K. Here, the surface mean roughness R is defined by the mean distance of the surface from a reference center plane with the average height, expressed as follows:

$$R=\frac{1}{L_x L_y}\int_0^{L_y}\int_0^{L_x} f(x,y)\,\mathrm{d}x\,\mathrm{d}y \qquad (2)$$

where $f(x,y)$ is the distance from the surface to the reference plane with average height, (x,y) the lateral coordinates along the surface, and L_x, L_y are the dimensions of the surface. A high value of R corresponds to a film surface morphology with many layers simultaneously exposed and a large fraction of layers with an individual height far away from the average height, giving a wide histogram of height distribution. In the plot of the film roughness three characteristic features are found and agree qualitatively very well with the three growth regions determined from MEED. At the initial stage of growth (region A, up to 2.5 ML) the high roughness corresponds to a pronounced

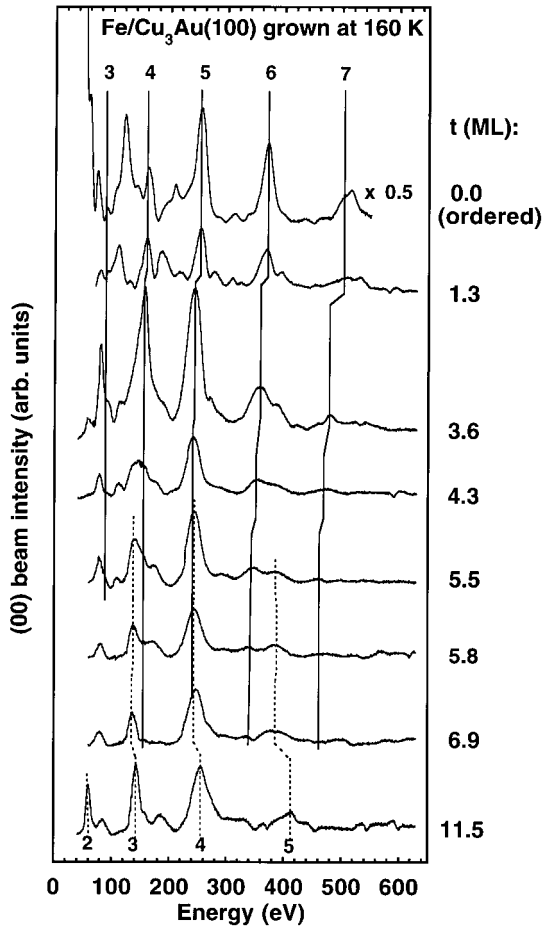

Fig. 16. LEED $I(E)$ curves of the (00) beam of the clean ordered $Cu_3Au(100)$ substrate and $Fe/Cu_3Au(100)$ grown at 160 K for various coverages. The solid and dashed lines indicate two different periodic peak sequences with the intensity weight depending on the thickness. The indices denote the integer numbers of the single scattering Bragg interference condition. Different from the case of growth at 300 K, the superposition of two peak sequences is observed at higher coverages from ~5.5 to 6.9 ML.

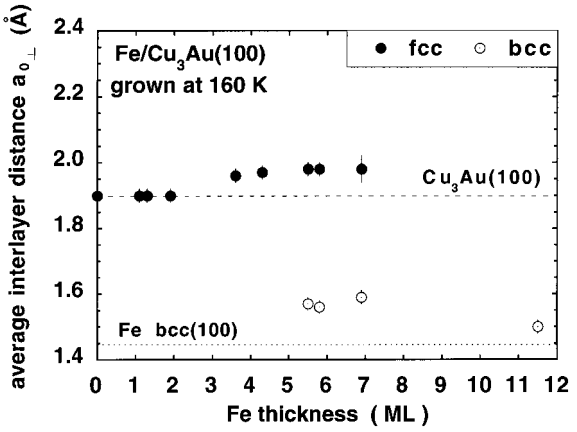

Fig. 17. Two different average vertical interlayer distance $a_\perp$ calculated from the $I(E)$ curves of Fig. 16 for the films grown at 160 K. They are related to fcc-like (full circles) and bcc-like Fe (open circles), respectively. The values of the vertical interlayer distance of the $Cu_3Au(100)$ substrate (measured) and bcc(100) Fe bulk (from literature) are indicated by horizontal lines. The onset of the growth of bcc-like Fe is delayed to a higher coverage of ~5.5 ML, as compared to growth at 300 K.

intensity drop in MEED. As shown in the STM images above (Fig. 3), Fe films at these coverages reveal a high island density. In region B (2.5–4.5 ML), one also finds two distinct oscillations in the roughness plot with minima at coverages of 3 and 4 ML, which have, however, still a much higher roughness than the clean $Cu_3Au(100)$ surface. The roughness (or MEED) oscillations with a periodicity of 1 ML are related to a layer-by-layer-like growth mode in Region B. Exhibiting this large average roughness (or small MEED specular intensity), the layer-by-layer-like film growth in region B should be connected in a complicated way to a multilayer or island growth mode. In region C, one can only observe very shallow oscillations with minima in the STM data (or maxima in the MEED data) in the vicinity of 5 and 6 ML. Finally, at higher coverages, the drop of the MEED specular intensity corresponds to a film morphology with a large roughness as observed in STM.

The quantitative relationship between the surface topology measured by STM and the diffraction intensity variations obtained by MEED is complex [30,31]. In the absence of a quantitative link between these two methods one still obtains a good qualitative agreement between the mean roughness in STM and the MEED specular intensity. Furthermore, this agreement also demonstrates a reproducible film quality of these samples prepared in different chambers for the two sets of measurements: Films grow at low coverage in a multilayer mode, from 3 to 4 ML in a quasi layer-by-layer mode (mixing of layer-by-layer and multilayer growth modes) and then go into the region

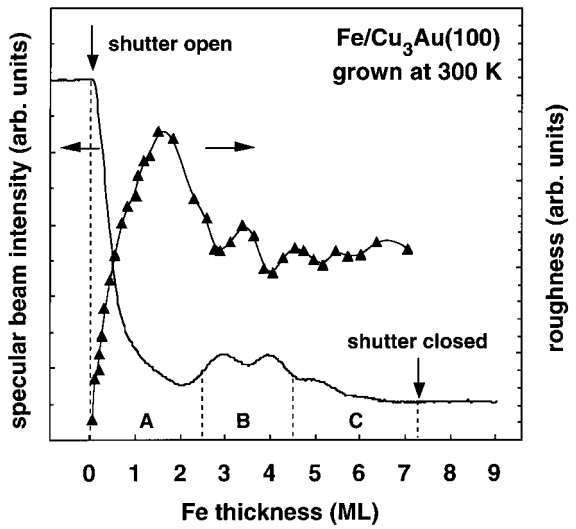

Fig. 18. Comparison of the surface mean roughness R (triangles), extracted from the STM measurements, and the MEED specular intensity during deposition (solid line) as a function of Fe thickness for Fe/Cu_3Au(100) films grown at 300 K. At the initial stage of growth (region A), the large surface mean roughness R corresponds to a pronounced intensity drop in MEED. In region B, both R and the MEED intensity reveal oscillations with a periodicity of 1 ML. The minima of R at coverages of 3 ML and 4 ML corresponds to the maximum of the MEED intensity. This agreement indicates also a reproducibility of the film quality of these samples prepared in different chambers for both STM and MEED measurements.

where the irregular Fe layers become predominant, the latter accompanied by a high surface roughness.

In contrast to growth at 300 K, we did not observe any MEED oscillations for growth at 160 K. The MEED specular intensity dropped drastically after starting the deposition. Together with the finding of higher number of the Fe islands in the STM images (Fig. 8), we can conclude that the growth at low temperature is far away from the layer-by-layer growth mode. Obviously, the growth temperature has a pronounced influence on the growth mode in our system, as is usually expected.

5.2. Morphology of Fe/Cu_3Au(100)

Besides the growth mode, another striking finding shown in Figs. 3 and 4 is the formation of the regularly shaped Fe (fcc-like) islands at coverages up to ~3.5 ML for films grown at 300 K. At these coverages Fe islands obviously prefer to grow along the in-plane ⟨011⟩ orientations, in contrast to the situation in the Fe/Cu(100) system, where a preferred orientation of island growth is not observed [22]. As indicated in Section 4.1, the influence of the different chemical configurations on the film growth and morphology is obscured in our films. The preferential growth orientation in the ⟨011⟩ direction should thus most likely be attributed to the enhanced mismatch strain rather than to the specific chemical configuration of the Cu–Au surface. Concerning the strain influence on island shape, Tersoff and Tromp [32] have reported that elongated islands allow better elastic relaxation of the stress rather than those with a compact shape. Thus a similar thermodynamic origin of the formation of the regular island shape may be suggested in our case.

We would now like to discuss briefly the origin of the network-like fine structure found in the 6.2 ML film grown at 160 K (Fig. 9). At first sight, such a network-like structure seems to be related to an accommodation mechanism acting by the formation of edge dislocations (or missing atoms) above a certain critical thickness owing to the lattice mismatch at the heterophase boundary. The distance between such dislocations can be expressed as [33,34]

$$s = \frac{ab}{|b-a|} \tag{3}$$

where a and b are the in-plane lattice parameters of the substrate and the overlayer, respectively. Using this formula and taking $a = 2.65$ Å for Cu_3Au(100) and $b = 2.53$ Å for fcc(100) Fe, Eq. (3) gives $s \approx 55$ Å. This value, however, is much higher than what we observe in Fig. 9 (the side of the unit mesh is only 7–14 Å). Thus, such a missing atom dislocation cannot be responsible for the observed network-like surface topology. More likely, some vertical buckling of adatoms (~0.2 Å height) with a lateral period of 3–5 atoms (i.e. 7–14 Å) along the close-packed orientation ⟨011⟩ may be the origin. A very similar square-grid network has been identified on thin film gold

bicrystal samples as a series of twist and/or tilt boundaries due to screw dislocations [35], where, in certain cases, the unit side of the network has found to be the order of 10 Å, being close to our observation.

5.3. Fcc–bcc structural transformation of $Fe/Cu_3Au(100)$ and comparison with Fe/Cu(100)

At room temperature, bulk bcc Fe has a lower free energy than bulk fcc Fe with a difference of the order of 0.018 eV atom^{-1} [36]. This energy difference usually determines the stable crystalline phase of a solid. According to this basic thermodynamic consideration of the free energy, a spontaneous fcc-to-bcc structural transformation of the Fe films should occur at a certain critical thickness. Such a transformation has indeed been observed in Fe films on Cu(100) [28,29,37], and in our case of $Fe/Cu_3Au(100)$ as shown above.

The structural transformation, however, is a rather complex crystallographic phenomenon. The crystal plane orientation in the final phase and the possible transformation path have been shown to be strongly dependent on the influence of the applied mechanical stress and the microchemistry [38]. Already in 1924 Bain [39] suggested that an fcc solid may transform spontaneously into a bcc or a bct (body-centered tetragonal) phase through relaxation of the interlayer spacing along the *c*-axis and biaxial expansion of the lattice constant along the $\langle 011 \rangle$ direction in the fcc (100) plane. Taking the *c*-axis as the direction normal to the film surface, such a ''Bain path'' transforms the fcc (100) into a bcc (or bct) (100) plane. The Bain deformation involves the minimal principal strain in the fcc–bcc (bct) transformation and is unique in that it maintains the highest crystal symmetry [40]. It is thus plausible to assume that in a heteropseudomorphic growth on an fcc(100) substrate, the fcc phase might be forced to transform into the bcc or bct phase owing to an enhanced misfit strain. This was observed even in a metal film for which the fcc phase is the stable phase in the bulk: As recently reported, an fcc-to-bct phase transition with increasing thickness in Cu films on Pd(100) takes place [41], which is driven along the Bain path by the total strain energy in the Cu film arising from the lattice mismatch (7.8%) for fcc Cu on Pd(100).

In our case, the fcc-like Fe film on $Cu_3Au(100)$ has a lattice mismatch of 4.2%. On the one hand, the large lattice mismatch, which induces the strain energy, and the (100) plane of the final bcc-like phase are comparable with those of the Cu/Pd(100) system. This strongly suggests that the Bain path via a *c*-axis contraction and a biaxial expansion is a possible transformation path in our case. On the other hand, a marked difference between the $Fe/Cu_3Au(100)$ system and Cu/Pd(100) is the large lattice mismatch between the bcc or bct (100) Fe and the $Cu_3Au(100)$ substrate ($\sim$7.3%). This could explain why the fcc-like underlayers in $Fe/Cu_3Au(100)$ or parts of them retain their fcc-like structure at least up to a certain coverage, even after the bcc-like Fe has started to grow on the topmost layer of films. It is thus also reasonable to assume that numerous dislocations (as shown in Fig. 4b and d), which accommodate the strain, occur at the interface between the fcc-like and the bcc-like phase. This makes it possible that the fcc-like underlayers or parts of them keep their structure at least up to a certain coverage without totally transforming into the bcc phase. This finding is different from that in Fe/Cu(100) films grown at room temperature, where the fcc–bcc structural transformation takes place in a martensitic (i.e. nondiffusive, collective and sudden) process involving complicated atomic rearrangements [28,29,42]. Such a martensitic transformation proceeds also into the deeper layers of the film down to the substrate [28,29,43]. This explains why Fe/Cu(100) films grown at 300 K which are only about one monolayer thicker than the critical thickness already reveal a predominant bcc(110) orientation in the LEED pattern and in the LEED $I(E)$ curves[4] [4,37] or in the STM images [29].

The surface orientation of bcc-like Fe on Cu(100) is (110), being different from the (100) orientation on $Cu_3Au(100)$. This can be more clearly understood by a comparison of the mismatch-induced strain energies between bcc(100)- or bcc(110)-oriented films and the $Cu_3Au(100)$ or Cu(100) substrates, respectively. Bcc Fe in the

[4] See footnote 1.

bulk has a nearest-neighbor spacing of 2.48 Å on a (110) and 2.87 Å on a (100) plane. The substrates Cu(100) and Cu_3Au(100) have a nearest-neighbor spacing of 2.55 and 2.65 Å along the surface, respectively. It is easy to see that bcc-like Fe films on Cu(100) with a (110) orientation have a smaller lattice mismatch than those with a bcc(100) orientation. Therefore, bcc Fe films on Cu(100) should prefer a final orientation of (110), according to this simple consideration on the lattice mismatch between the final state and the substrate. Furthermore, fcc(100) Fe films on Cu(100) have a mismatch of only 1%, which is much smaller than the 4.2% of fcc(100) Fe films on Cu_3Au(100). This may lead to the absence of a large mismatch-induced strain energy in fcc Fe/Cu(100), which is the necessary driving force for a Bain path[5]. Hence, this may be one of the reasons that, instead of a Bain transformation, the fcc–bcc structural transformation of Fe/Cu(100) takes place through some kind of shear displacement.

In contrast to Fe/Cu(100), the value of the nearest-neighbor spacing of Cu_3Au(100) lies almost midway between those of the Fe bcc(100) and the bcc(110) phase. Hence, the lattice mismatch of bcc(100) Fe on Cu_3Au(100) is comparable with that of bcc(110) Fe. Based only on this aspect, a preferred final orientation of bcc-like Fe may not be defined. Thus, the large mismatch-induced strain energy between the fcc(100) Fe and Cu_3Au(100) may be the decisive factor to determine the transformation path and the final orientation of the bcc-like Fe film. This argument suggests that in the Fe/Cu_3Au(100) system a structural transformation from fcc(100) into bcc(100) is driven by this lattice mismatch-induced strain through a simple Bain path (i.e. without further complicated rigid lattice rotation).

5.4. *Effect of structural transformation and roughness on magnetic properties*

As mentioned in Section 1, Fe/Cu_3Au(100) provides a magnetic film system with stable magnetic phase, permitting us to study the effect of structure and morphology on the magnetic anisotropy. In our magnetic measurements [7,8] using the magneto-optical Kerr effect the magnetization of Fe/Cu_3Au(100) at 160 K reveal the easy axis perpendicular to the film surface at coverages up to 3.5 ML and 5.5 ML for growth at 300 K and 160 K, respectively. On increasing the film thickness, the magnetization continuously switches into the in-plane direction within a narrow thickness range of $\sim$0.5 ML. The critical thickness of the spin reorientation transition is thus determined to be 3.5 and 5.5 ML for growth at 300 and 160 K, respectively.

Based on this magnetic information, we found that the spin reorientation transition is correlated with the fcc–bcc structural transformation, which was also shown to appear at a coverage close to the critical thickness for both growth temperatures. The growth of bcc-like Fe seems to have a decisive influence on the magnetic anisotropy in this system. An enhanced magnetocrystalline surface anisotropy was considered to be responsible for the existence of a perpendicular magnetization in many systems, such as Fe/Ag(100) [44] and Fe/Cu(100) [45,46] as well as the present system [7]. Since the enhancement of the magnetocrystalline surface anisotropy is mainly attributed to the broken symmetry at surfaces and interfaces, as originally suggested by Néel [47], it must be very sensitive to the quality of the film surface. As shown in our structural data above, the structural transformation is accompanied by a large number of dislocations and structural defects at the film surface, leading to a poor crystalline structure. This may drastically reduce the magnetocrystalline surface anisotropy or the perpendicular anisotropy, resulting in the spin reorientation transition in the present case.

Besides the magnetocrystalline surface anisotropy, in a measurement of the effective anisotropy field a perpendicular volume anisotropy due to the vertical lattice distortion has recently been reported to make the main contribution to the perpendicular magnetization for the Fe/Cu(100 system [48]. A structural transformation from fct to bcc phase reduces the value of this volume anisotropy close to unstrained bulk bcc Fe.

[5] The Bain transformation can reach not only a bcc(100) plane but also a bcc(110). A combination of the Bain path and a rigid lattice rotation can also reach a bcc(110) plane from an fcc(100) plane.

In the absence of a direct measurement of the magnetic anisotropy, we do not know the role of the volume anisotropy suggested in Ref. [48] in Fe/Cu_3Au(100). Nevertheless, according to the above discussion, both the magnetic surface anisotropy and the distortion-induced (magneto-elastic) volume anisotropy, and thus the perpendicular magnetic anisotropy of the system, are expected to be drastically reduced through the fcc–bcc structural transformation. The spin reorientation transition in Fe/Cu_3Au(100) is then induced by this reduction of the perpendicular magnetic anisotropy.

Finally, we would like to make a brief remark on the effect of the surface roughness on the magnetic anisotropy. Taking the roughness extracted from our STM data and using the theory developed by Bruno [49,50] based on the Néel model, an estimation of the roughness-related change in magnetic anisotropy for Fe/Cu_3Au(100) shows that this effect is not strong enough to induce the spin reorientation transition and is thus only of little importance. A detailed study of magnetism and its correlation to structural transformation and morphology is reported elsewhere [8].

6. Summary

We have studied the growth mode, surface morphology, and crystalline structure of Fe films on Cu_3Au(100) for different growth temperatures using STM and LEED. Fe/Cu_3Au(100) films grown at 300 K start with a multilayer growth up to $\sim$2.5 ML, and proceed with ''quasi-layer-by-layer'' growth up to $\sim$5 ML. The absence of the layer-by-layer growth mode which was found in Fe/Cu(100) grown at 300 K [22,46] is attributed to the enhanced strain due to the large lattice mismatch (4.2%) between fcc Fe and the Cu_3Au(100) substrate. Fe/Cu_3Au(100) films grown at 160 K reveal only multilayer growth, being similar to Fe/Cu(100) films grown at low temperatures.

For growth at 300 K, Fe islands grow, up to a coverage of $\sim$3.5 ML, in a regular shape with a preferred $\langle 110 \rangle$ edge orientation. The tendency of the island growth at 160 K towards to a preferential orientation, however, is much weaker, as compared with growth at 300 K. At coverages around 6 ML, films grown at 160 K have a nearly closed layer, however, with a fine network structure. This network structure is expected to be due to a vertical buckling of atoms rather than to some missing atom dislocation caused by the lattice mismatch.

The onset of the fcc–bcc structural transformation in Fe/Cu_3Au(100) is, according to both LEED $I(E)$ and STM measurements, found to be 3.5 and 5.5 ML for growth at 300 and 160 K, respectively. The bcc-like Fe grows on the top of the film surface and covers the fcc-like Fe underlayers, which seem to retain their fcc-like structure up to higher coverages. The final orientation of the bcc-like Fe is (100), rather than (110) found in the Fe/Cu(100) system. This final bcc(100) phase is most likely reached through the Bain path.

Our findings demonstrate the strong influence of a substrate with an enhanced lattice mismatch on the growth mode as well as on the surface topography such as the shape of islands, as compared with the Fe/Cu(100) system. The path of the structural transformation and the orientation of transformed bcc-like Fe should also take the effect of the mismatch-induced strain into account. The growth temperature is shown to be another important factor which affects the surface morphology of the film. The presence of island growth is usually expected for growth at low temperatures owing to the reduced mobility of adatoms. Nevertheless, the striking finding of a nearly closed layer with a fine network structure in the film grown at 160 K indicates that a more complicated mechanism in the film growth must be involved in this system. A deeper understanding of this finding needs further experimental and theoretical study.

Our structural and morphological investigations in the present paper provide a basis set of data for studying the possible influence of structure and morphology on the magnetic properties. The fcc–bcc structural transformation is shown to be interrelated to the spin reorientation transition from a perpendicular into an in-plane direction. The effect of the surface roughness on the spin reorientation transition is, within the theoretical

model by Bruno [49,50], negligible as far as the spin reorientation transition is concerned.

Note added in proof

After submission we became aware of another publication about $Fe/Cu_3Au(100)$ (Feldmann et al., Phys. Rev. B 57 (1998) 1014).

Acknowledgements

The authors would like to thank Dr. J. Giergiel for helpful discussions, and B. Zada and F. Pabisch for their expert technical support. This work was supported by the Deutsche Forschungsgemeinschaft under Grant No. Schn353/3.

References

[1] G.L. Krasko, G.B. Olson, J. Appl. Phys. 67 (1990) 4570.
[2] V.L. Moruzzi, P.M. Marcus, K. Schwarz, P. Mohn, Phys. Rev. B 34 (1986) 1784.
[3] D.J. Keavney, D.F. Storm, J.W. Freeland, I.L. Grigorov, J.C. Walker, Phys. Rev. Lett. 74 (1995) 4531.
[4] S. Müller, P. Bayer, C. Reischl, K. Heinz, B. Feldmann, H. Zillgen, M. Wuttig, Phys. Rev. Lett. 74 (1995) 765.
[5] R.D. Ellerbrock, A. Fuest, A. Schatz, W. Keune, R.A. Brand, Phys. Rev. Lett. 74 (1995) 3053.
[6] S.H. Lu, J. Quinn, D. Tian, F. Jona, P.M. Marcus, Surf. Sci. 209 (1989) 364.
[7] F. Baudelet, M.-T. Lin, W. Kuch, K. Meinel, B. Choi, C.M. Schneider, J. Kirschner, Phys. Rev. B 51 (1995) 12563.
[8] M.-T. Lin, J. Shen, W. Kuch, H. Jenniches, M. Klaua, C.M. Schneider, J. Kirschner, Phys. Rev. B 55 (1997) 5886.
[9] A.K. Schmid, J. Kirschner, J. Vac. Sci. Technol. B 49 (1991) 649.
[10] M.-T. Lin, J. Shen, W. Kuch, C.M. Schneider, J. Kirschner, unpublished.
[11] M. Zharnikov, A. Dittschar, W. Kuch, C.M. Schneider, J. Kirschner, Phys. Rev. Lett. 76 (1996) 4620.
[12] M. Zharnikov, A. Dittschar, W. Kuch, C.M. Schneider, J. Kirschner, J. Magn. Magn. Mater. 174 (1997) 40.
[13] R. Smoluchowski, in: E.U. Condon et al. (Eds.), Handbook of Physics, McGraw-Hill, New York, 1967, pp. 8–97.
[14] T.M. Buck, G.H. Wheatley, L. Marchut, Phys. Rev. Lett. 51 (1983) 43.
[15] H. Niehus, C. Achete, Surf. Sci. 289 (1993) 19.
[16] H.M. Polatoglou, unpublished.
[17] K.R. Mecke, S. Dietrich, Phys. Rev. B 52 (1995) 2107.
[18] H. Reichert, P.J. Eng, H. Dosch, I.K. Robinson, Phys. Rev. Lett. 74 (1995) 2006.
[19] W.B. Pearson, A Handbook of Lattice Spacings and Structures of Metals and Alloys, Pergamon, New York, 1967.
[20] L.Z. Mezey, J. Giber, Jpn. J. Appl. Phys. 21 (1982) 1569.
[21] W.A. Jesser, J.W. Mattews, Philos. Mag. 17 (1968) 595.
[22] J. Giergiel, J. Shen, J. Woltersdorf, A. Kirilyuk, J. Kirschner, Phys. Rev. B 52 (1995) 8528.
[23] A. Dittschar, M. Zharnikov, W. Kuch, C.M. Schneider, J. Kirschner, unpublished.
[24] J.B. Pendry, Low Energy Electron Diffraction, Academic Press, New York, 1974.
[25] P. Jiang, P.M. Marcus, F. Jona, Solid State Commun. 59 (1986) 275.
[26] V.L. Moruzzi, P.M. Marcus, J. Kübler, Phys. Rev. B 39 (1989) 6957.
[27] G.L. Krasko, G.B. Olson, Phys. Rev. B 40 (1989) 11536.
[28] K. Kalki, D.D. Chambliss, K.E. Johnson, R.J. Wilson, S. Chiang, Phys. Rev. B 48 (1993) 18344.
[29] J. Giergiel, J. Kirschner, J. Landgraf, J. Shen, J. Woltersdorf, Surf. Sci. 310 (1994) 1.
[30] D.D. Chambliss, K.E. Johnson, Surf. Sci. 313 (1994) 215.
[31] J.A. Stroscio, D.T. Pierce, R.A. Dragoset, Phys. Rev. Lett. 70 (1993) 3615.
[32] J. Tersoff, R.M. Tromp, Phys. Rev. Lett. 70 (1993) 2782.
[33] H. Lüth, Surfaces and Interfaces of Solid Materials, Springer, Berlin, 1995.
[34] K.-N. Tu, J.W. Mayer, L.C. Feldman, Electronic Thin Film Science, Macmillan, New York, 1992.
[35] R.W. Balluffi, Y. Komem, T. Schober, Surf. Sci. 31 (1972) 68.
[36] K.S. Cheung, R.J. Harrison, J. Appl. Phys. 71 (1992) 4009.
[37] M. Wuttig, B. Feldmann, J. Thomassen, F. May, H. Zillgen, A. Brodde, H. Hannemann, H. Neddermeyer, Surf. Sci. 291 (1993) 14.
[38] H. Schumann, Crystal Geometry: Theory of Lattice Transformation, DVG, Leipzig, 1980.
[39] E.C. Bain, Trans. AIME 70 (1924) 25.
[40] F. Milstein, B. Farber, Phys. Rev. Lett. 44 (1980) 277.
[41] E. Hahn, E. Kampshoff, N. Wälchli, K. Kern, Phys. Rev. Lett. 74 (1995) 1803.
[42] P. Schmailzl, K. Schmidt, P. Bayer, R. Doell, K. Heinz, Surf. Sci. 312 (1994) 73.
[43] J. Koike, M. Nastasi, in: C.V. Thompson et al. (Eds.), Evolution of Thin Films and Surface Microstructure, MRS Symposia, Material Research Society, Pittsburg, PA, 1991, pp. 13.
[44] Z.Q. Qiu, J. Pearson, S.D. Bader, Phys. Rev. Lett. 70 (1993) 1006.
[45] D.P. Pappas, K.-P. Kämper, H. Hopster, Phys. Rev. Lett. 64 (1990) 3179.
[46] J. Thomassen, F. May, B. Feldmann, M. Wuttig, H. Ibach, Phys. Rev. Lett. 69 (1992) 3831.
[47] L. Néel, J. Phys. Radium 15 (1954) 376.
[48] D.E. Fowler, J.V. Barth, Phys. Rev. B 53 (1996) 5563.
[49] P. Bruno, J. Phys. F 18 (1988) 1291.
[50] P. Bruno, J. Appl. Phys. 64 (1988) 3153.